Regenerative Biomedicine

Production and Hosting: Shahid Sadoughi University of Medical Sciences

Journal homepage: jrb.ssu.ac.ir

Original Article

Investigation of the Release of Linagliptin from an Injectable Sodium Alginate/Gelatin Hydrogel in a Physiological Environment (in vitro)

Mohammad Amin Kouchakzade [1], Yaser Ghelmani [1*], Vahid Ramezani [2], Fatemeh Kuchakzade [3], Habib Nikukar [3], Akram Ghadiri-Anari [4]

1- Faculty of Internal Medicine, Shahid-Sadoughi University of Medical Sciences, Yazd, Iran.

2- Department of Pharmaceutics, Faculty of Pharmacy, Shahid Sadoughi University of Medical Sciences, Yazd, Iran.

3- Biotechnology Research Center, Yazd Reproductive Sciences Institute, Shahid Sadoughi University of Medical Sciences, Yazd, Iran.

4- Diabetes Research Center, Shahid Sadoughi University of Medical Sciences, Yazd, Iran.

***Corresponding Author:**
Yaser Ghelmani

Email:
y.ghelmani@ssu.ac.ir

Received:
2026-02-16
Revised:
2026-06-12
Accepted:
2026-06-20

Volume:2
Issue no.1

Copyright © 2025 The Authors.
This work is licensed under a Creative Commons Attribution 4.0 International License, which permits unrestricted use, distribution, and reproduction in any medium, provided the original work is properly cited.

Abstract

Diabetes mellitus affects approximately 422 million people worldwide, with prevalence projected to double within two decades. Linagliptin, a dipeptidyl peptidase-4 inhibitor utilized for type 2 diabetes management, exhibits limited oral bioavailability (29.5%) due to extensive first-pass metabolism, necessitating alternative drug delivery strategies. An injectable drug delivery system for linagliptin, a type 2 diabetes management drug was developed through the synthesis of an alginate/gelatin hydrogel. The hydrogel underwent testing to assess its hydrating behavior, material breakdown, ability to be injected, and its crosslinking characteristics using FTIR and XRD testing methods. The hydrogel showed moderate swelling behavior with minimal tissue damage potential and a degradation time of one month which made it suitable for use in drug delivery systems. The hydrogel exhibited rheological properties that were controlled by temperature because it underwent a sol-gel transition at the temperature of 37 degrees Celsius because FTIR and XRD tests showed that crosslinking had been achieved. The drug release profile demonstrated an initial burst effect at 30 minutes which was followed by a sustained release pattern. The developed alginate/gelatin hydrogel represents a promising candidate for sustained linagliptin delivery, exhibiting slow degradation, moderate swelling, and favorable injectability. These properties suggest potential for reducing dosing frequency compared to conventional oral administration, pending validation through in vivo studies.

Keywords: Alginate-gelatin, Injectable hydrogel, Linagliptin, Sustained release, Type 2 diabetes

How to cite this article:
Kouchakzade, MA., Ghelmani, Y., Ramezani, V., Kuchakzade, F., Nikukar, H., Ghadiri-Anari, A. Investigation of the release of linagliptin from an injectable sodium alginate/gelatin hydrogel in a physiological environment (in vitro). *Regenerative Biomedicine*, 2026; 2(1): 20-42. https://doi.org/10.22034/jrb.2026.07.V2I1A2

Introduction

Diabetes mellitus is a metabolic disorder characterized by hyperglycemia resulting from impaired insulin secretion and/or insulin resistance (1). The global burden has escalated dramatically, rising from 30 million cases in 1985 to over 463 million in 2019, with projections indicating 640 million affected individuals by 2040 (2, 3). Type 2 diabetes mellitus (T2DM) predominates, with prevalence anticipated to increase from 5.9% in 2021 to 9.5% by 2050, potentially affecting 1.2 billion people (4, 5). This growing epidemic imposes substantial health and economic consequences, accounting for 11% of adult deaths and projected health costs rising from 760billiontoover1,000 billion annually by 2045 (6-8). Regional variations are evident, with systematic reviews in Iran reporting approximately 10.8% prevalence among adults aged 25 and over, reaching 15.3% in Khuzestan Province and 14.4% in Khorasan Razavi Province (9). Pharmacological management of T2DM frequently involves dipeptidyl peptidase-4 (DPP-4) inhibitors, which prevent incretin hormone degradation, thereby enhancing glucose-dependent insulin secretion while suppressing glucagon release (10-12). Linagliptin, a prominent agent in this class, exhibits favorable pharmacokinetics including a long half-life and predominant non-renal elimination, which eliminates dose adjustment requirements in hepatic or renal impairment (13-15). However, clinical utility is constrained by limited oral bioavailability (29.5%) attributable to extensive first-pass hepatic and intestinal metabolism, necessitating daily administration (16). To address these limitations, various controlled-release formulations have been investigated, including matrix-based tablets, nanoparticulate carriers, and lipid-based systems designed to prolong drug release and maintain constant plasma levels (17-19). While these approaches demonstrate improved pharmacokinetics compared to immediate-release formulations, significant limitations persist. Many conventional matrix tablets exhibit burst release phenomena or incomplete protection from first-pass metabolism, whereas nanoparticulate systems often suffer from rapid clearance, manufacturing complexities, or insufficient duration of sustained delivery. Furthermore, the oral route inherently suffers from incomplete absorption and fluctuating plasma concentrations (20). Consequently, parenteral depot systems, particularly injectable hydrogels that bypass hepatic first-pass effects while providing tunable, sustained release kinetics, have garnered substantial attention as alternative platforms (21). Among biomaterial options, alginate-gelatin composites have emerged as promising scaffolds for controlled drug delivery (22). Alginate, a natural polysaccharide, forms stable ionic crosslinks with divalent cations to create gel structures with controllable porosity, while gelatin enhances mechanical strength, flexibility, and biocompatibility (23, 24). These polymers synergistically create a flexible matrix capable of maintaining therapeutic drug concentrations for extended periods (25). Previous investigations have established the general utility of alginate-gelatin hydrogels for various pharmaceutical applications, demonstrating their capacity for sustained release of diverse therapeutic agents. However, critical gaps remain regarding their optimization for injectable linagliptin

OPEN ACCESS

delivery. Specifically, existing studies lack comprehensive characterization of dual-crosslinked networks combining Schiff base chemistry with ionic interactions, detailed rheological profiling including oscillatory analyses and linear viscoelastic verification, and systematic evaluation of injectability through clinically relevant needle gauges. Moreover, quantitative assessment of swelling kinetics and degradation profiles specifically tailored for sustained DPP-4 inhibitor release remains inadequately addressed.

The present study addresses these deficiencies by developing a dual-crosslinked alginate-gelatin hydrogel specifically engineered for linagliptin encapsulation and sustained release. Unlike previous systems that relied solely on ionic crosslinking or lacked comprehensive injectability assessment, this work introduces an optimized dual-crosslinking strategy that enhances mechanical resilience while maintaining injectability. The objective was to synthesize and comprehensively characterize an injectable depot system, evaluating its physicochemical properties, rheological behavior, injectability, and in vitro release kinetics. This approach offers a novel strategy to overcome the low oral bioavailability and frequent dosing limitations associated with conventional linagliptin administration.

Materials and Methods

Materials

Linagliptin in its pure form was obtained from Kharazmi Pharmaceutical Company (Tehran, Iran). Sodium alginate (medium viscosity), gelatin (Type B, 225 Bloom), calcium chloride dihydrate ($CaCl_2 \cdot 2H_2O$), microbial transglutaminase enzyme (100 U/g), and phosphate-buffered saline (PBS, pH 7.4) were purchased from Sigma-Aldrich (USA). All other reagents were of analytical grade and used directly without further purification.

Preparation of Alginate/Gelatin Injectable Hydrogel

To prepare the injectable hydrogel, 500 mg sodium alginate was dissolved in 5 mL distilled water at room temperature under gentle stirring. Separately, 500 mg gelatin was dissolved in 5 mL PBS (pH 7.4) at 40°C. Subsequently, 50 mg transglutaminase enzyme (dissolved in 2 mL distilled water) was added to the gelatin solution under light stirring, followed by slow incorporation of the alginate solution. Finally, either 15 or 30 µL of 0.1 M $CaCl_2$ solution was added dropwise under continuous stirring (600 rpm) to achieve dual crosslinking. The mixture was incubated at 37°C for 24 hours to complete ionic crosslinking and enzymatic gelation (26).

Drug Loading and Encapsulation Efficiency

We integrated linagliptin into the polymer blend right before introducing the calcium chloride. Drawing from pharmacokinetic insights, each hydrogel sample received 10.325 mg of linagliptin, calibrated to support steady release across seven days. To gauge encapsulation efficiency, we measured the free drug lingering in the supernatant post-gelation, via UV–Vis spectrophotometry at a 295 nm wavelength.

Experimental Design

Four distinct formulations were prepared and characterized: (a) blank hydrogel with 15 µL $CaCl_2$ (H(15)), (b) blank hydrogel with 30 µL

https://doi.org/10.22034/jrb.2026.07.V2I1A2

$CaCl_2$ (H(30)), © linagliptin-loaded hydrogel with 15 µL $CaCl_2$ (L+H(15)), and (d) linagliptin-loaded hydrogel with 30 µL $CaCl_2$ (L+H(30)). All experiments were conducted in triplicate (n = 3) unless otherwise specified, with results expressed as mean ± standard deviation (SD) (27, 28).

Swelling and Degradation Study

For swelling studies, pre-weighed dry hydrogels (W_0) were immersed in PBS (pH 7.4) at 37°C for 24 hours. After removal, surface moisture was gently blotted with filter paper, and swollen weights (W_t) were recorded. The swelling degree was calculated as:

$$Swelling\ (\%) = \frac{W_t - W_0}{W_0} \times 100$$

For degradation studies, hydrogels were incubated in PBS (pH 7.4) at 37°C for up to 30 days. At predetermined time intervals, samples were retrieved, rinsed with distilled water, lyophilized, and weighed (W_t). Weight loss percentage was calculated as:

$$Degradation\ (\%) = \frac{W_0 - W_t}{W_0} \times 100$$

Each experiment was performed in triplicate (n = 3) (26).

Injectability Test

Injectability was assessed by extruding freshly prepared hydrogels through standard syringes (1 mL) fitted with 23G, 25G, and 27G needles at 37°C. We gauged injection smoothness and flow consistency on a qualitative basis. Tests were performed in triplicate (n = 3) for each formulation (28).

Rheological Characterization

Rheological properties were investigated using a modular rheometer (MCR 302, Anton Paar, Austria) equipped with a cone-and-plate geometry (50 mm diameter, 1° cone angle, 0.1 mm gap). Oscillatory temperature sweep tests were performed from 10°C to 40°C at a heating rate of 2°C/min to monitor sol–gel transition. Measurements were conducted at a constant frequency of 1 Hz and strain amplitude of 1%, which was confirmed to be within the linear viscoelastic region (LVER) through preliminary amplitude sweep tests (0.1–10% strain at 25°C). Frequency sweep tests (0.1–10 Hz) were performed at 37°C to evaluate gel stability. For all formulations (H(15), H(30), L+H(15), and L+H(30)), the following parameters were recorded: storage modulus (G^'), loss modulus (G^''), loss tangent (tan⁡δ=G^''/G^'), and complex viscosity $\eta^* = \sqrt{(G')^2 + (G'')^2}/\omega$, where ωis the angular frequency in rad/s). All rheological measurements were performed in triplicate (n = 3) (26).

Fourier-Transform Infrared Spectroscopy (FT-IR) Analysis

FT-IR spectra were recorded using a Nicolet iS10 spectrometer (Thermo Scientific, USA) in the range of 4000–650 cm^{-1} with a resolution of 4 cm^{-1} using attenuated total reflectance (ATR) mode. Spectra were obtained for pure alginate, pure gelatin, linagliptin powder, blank hydrogels (H(15) and H(30)), and drug-loaded hydrogels (L+H(15) and L+H(30)). All spectra are presented as overlaid plots to enable direct comparison of peak shifts and intensity changes indicative of chemical interactions (29).

X-Ray Diffraction (XRD) Analysis

XRD patterns were collected using a Bruker D8 Discover diffractometer (Germany) with Cu Kα radiation (λ = 1.5406 Å) operating at 35 kV and 35 mA. Samples were scanned from 10° to 80° (2θ) at a rate of 4°/min. Data were analyzed using Bruker Eva software to assess crystallinity changes. Diffractograms of pure linagliptin, blank hydrogel, and drug-loaded hydrogels are presented as overlaid plots for comparative analysis of molecular dispersion (30).

In Vitro Drug Release Study

Drug release was evaluated using the dialysis bag method. Hydrogel samples (1 mL) were placed in dialysis membranes (MWCO 12–14 kDa, pore size 3.5–5 nm) and immersed in 200 mL PBS (pH 7.4) at 37 ± 0.5°C under gentle agitation (50 rpm). At predetermined time intervals (1, 3, 6, 12, 24, 48 h, and every 24 h thereafter), 2 mL aliquots were withdrawn and replaced with fresh PBS to maintain sink conditions. Linagliptin concentration was determined by UV–Vis spectrophotometry at 295 nm using a calibration curve $R^2 > 0.999$. Cumulative drug release was calculated using the Beer–Lambert law. All release experiments were performed in triplicate (n = 3), and results are reported as mean ± SD (31).

Statistical Analysis

All data are presented as mean ± standard deviation (SD) from three independent experiments (n = 3). Statistical analyses were performed using one-way analysis of variance (ANOVA) followed by Tukey's post-hoc test for multiple comparisons between groups. Statistical significance was set at $p < 0.05$. All calculations were conducted using GraphPad Prism software (version 9.0, GraphPad Software, USA).

Results

Swelling Behavior

The four hydrogel formulations L+H(30), H(30), L+H(15), and H(15) underwent testing to determine their equilibrium swelling ratios after immersion in phosphate-buffered saline (PBS, pH 7.4) at 37 ± 0.5°C for 24 h. As illustrated in Figure 3-1, all formulations exhibited high fluid absorption capacity because their porous network structure and hydrophilic polymer systems enabled substantial liquid uptake. The equilibrium swelling percentages were quantified as follows: H(15) exhibited 3.36±0.12%, H(30) demonstrated 8.75±0.24%, L+H(15) showed 3.31±0.17%, and L+H(30) achieved 7.74±0.23%(mean ±SD, n=3).

Statistical analysis using one-way ANOVA confirmed that H(30) exhibited significantly higher water absorption capacity than H(15) ($p<0.001$), attributed to the fact that higher polymer concentrations result in improved water retention performance. This occurrence emerges from hydrophilic functional groups at high polymer concentrations creating more hydrogen bonding sites (−OH, $-NH_2$, $-COO^-$) which form bonds with water molecules, thereby enhancing the thermodynamic compatibility between the polymer network and aqueous medium. The drug-loaded formulations (L+H groups) showed statistically significant decreases in swelling ratios compared to their drug-free counterparts (L+H(15) vs. H(15): $p<0.01$; L+H(30) vs. H(30): $p<0.05$). This reduction occurs because linagliptin molecules create physical entanglements with polymer chains through hydrogen bonding and hydrophobic

https://doi.org/10.22034/jrb.2026.07.V2I1A2

interactions that restrict polymer segmental mobility and decrease water absorption potential. According to the Flory-Rehner theory, the incorporation of solutes within the polymer network alters the thermodynamic equilibrium between the elastic retractive forces of the polymer network and the osmotic pressure driving water influx, resulting in reduced equilibrium swelling.

Degradation Rate

The hydrogel formulations underwent biodegradation testing using gravimetric measurements in PBS (pH 7.4) at 37°C for 30 days (Figure 3-2). All samples exhibited mass increase during the first 24 h due to hydration as the polymer network absorbed water, followed by initiation of hydrolytic degradation. After the initial hydration period, formulations began to lose mass progressively as hydrolytic cleavage of glycosidic and amide bonds occurred within the polymer backbone. By day 30, formulations H(15), L+H(15), and L+H(30) reached complete degradation (100±0% weight loss), whereas H(30) retained 11.62±0.20%of its original mass, achieving 88.38±0.32%degradation (mean ±SD, n=3).

Two primary elements determine the different degradation rates observed: (i) crosslinking density dependence on polymer concentration, and (ii) drug-polymer interactions. Statistical analysis confirmed that H(30) degraded significantly slower than H(15) at day 30 ($p<0.001$), as its higher polymer concentration leads to increased crosslinking density that creates physical entanglements, developing a robust network that prevents hydrolytic cleavage. Consistent with established literature on biodegradable hydrogels, higher crosslinking densities correlate with slower degradation rates due to reduced accessibility of water molecules to cleavable bonds. Interestingly, the presence of linagliptin significantly accelerated the degradation process, as evidenced by L+H(30) achieving complete degradation while H(30) remained partially undegraded (L+H(30) vs. H(30): $p<0.01$at day 30). This phenomenon occurs because: (a) the drug-loaded matrix becomes more hydrophilic, facilitating water ingress into the system, and (b) the drug functional groups may act as hydrolysis catalysts or induce less organized polymer chain conformations, creating additional sites susceptible to hydrolytic attack.

Injectability

The hydrogel formulations underwent injectability assessment using standard hypodermic needles of varying gauges (23G, 25G, 27G, and 30G; inner diameters of 0.337 mm, 0.260 mm, 0.210 mm, and 0.160 mm, respectively). Qualitative assessment ($n = 3$ injections per formulation) revealed distinct flow behaviors dependent on formulation viscosity and needle diameter.

The high-concentration formulations [L+H(30) and H(30)] produced smooth and continuous extrusion through 23G needles without requiring excessive force (<10 N) or encountering syringe blockage. These hydrogels exhibited pronounced shear-thinning behavior, described by the power-law relationship $\eta = K \cdot \dot{\gamma}^{n-1}$ where $n < 1$, enabling them to flow when pressure was applied despite their high zero-shear viscosity. This rheological profile necessitated larger bore diameters to maintain injection forces below the clinically acceptable limit of

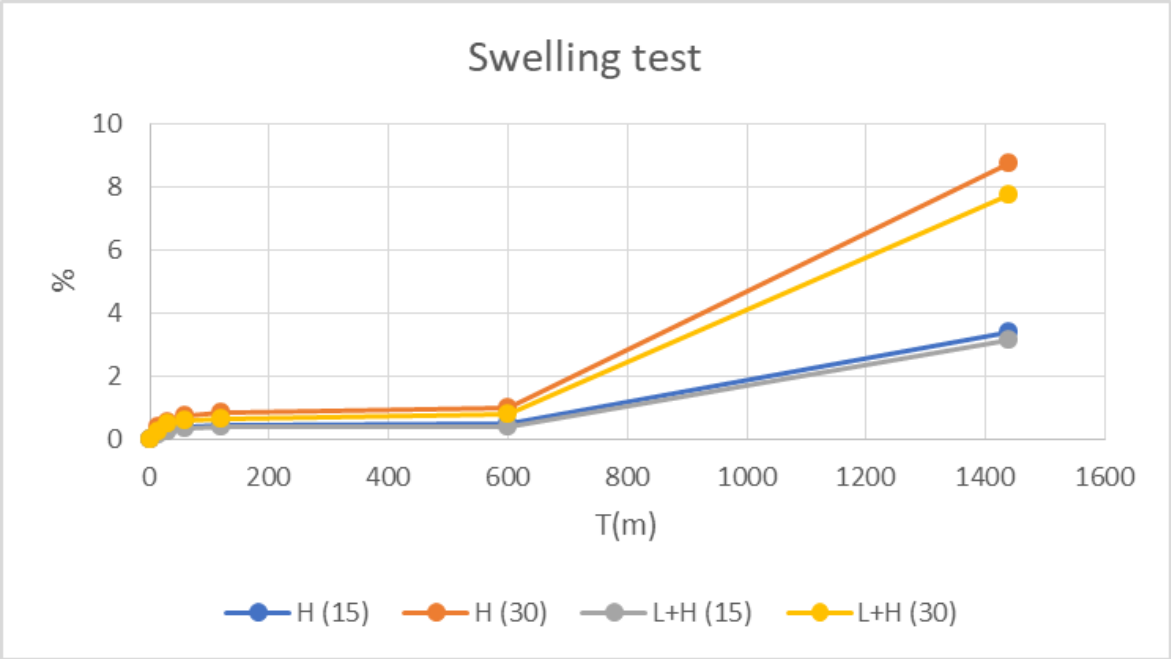


Figure 1. Equilibrium swelling ratios of hydrogel formulations in PBS at 37°C. Data represent mean ±standard deviation (n = 3). H: hydrogel; L: linagliptin.

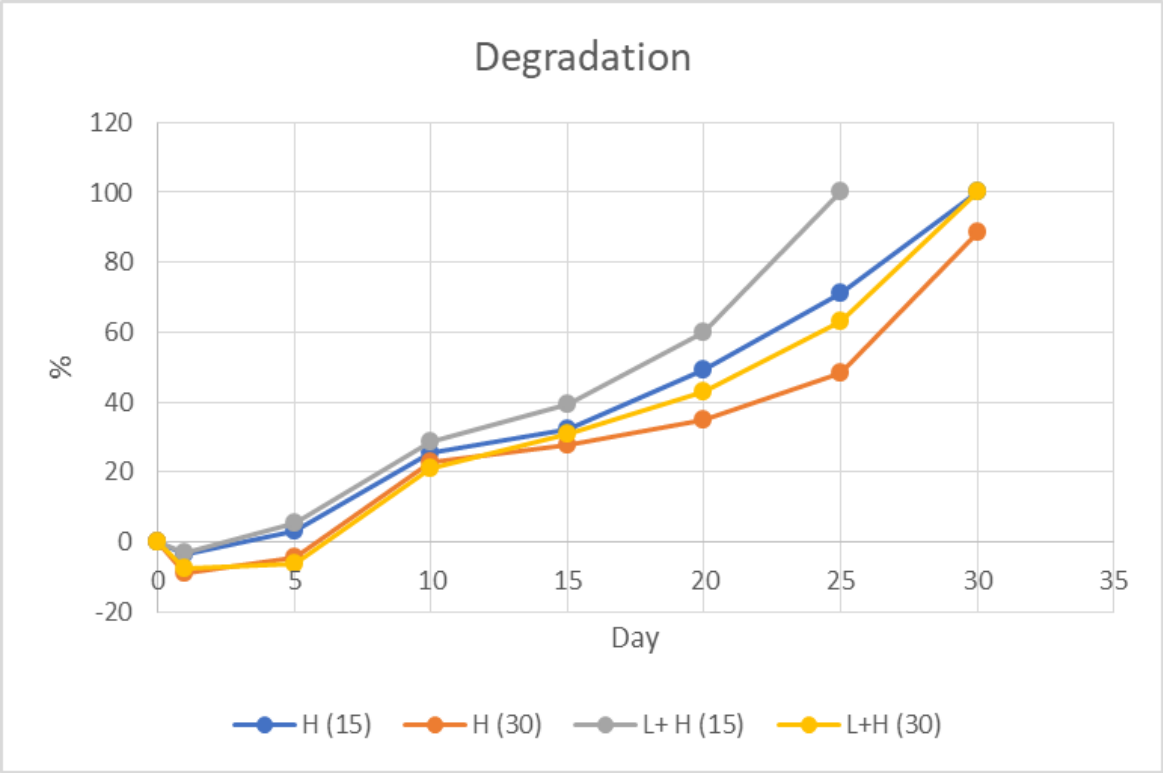


Figure 2. Cumulative degradation profiles of hydrogel formulations in PBS (pH 7.4) at 37°Cover 30 days. Data represent mean ±standard deviation (n = 3). H: hydrogel; L: linagliptin.

https://doi.org/10.22034/jrb.2026.07.V2I1A2

20 N. Conversely, the low-concentration formulations [L+H(15) and H(15)] demonstrated optimal injectability through 25G needles, providing an optimal balance between ease of injection and minimal tissue trauma. Attempts to pass H(30) through 30G needles resulted in blockage due to the high elastic modulus ($G' > 1000$ Pa), whereas H(15) could be extruded through 27G needles with moderate force. These findings demonstrate that needle gauge selection must be tailored to the rheological properties of the specific formulation, as higher viscosity systems require larger needle gauges to maintain proper flow while protecting the hydrogel microstructure from shear-induced damage during administration.

Viscosity

The viscoelastic properties of hydrogel formulations were characterized using oscillatory rheometry at 25°Cand 37°Cto simulate room temperature and physiological conditions. Temperature sweep experiments (frequency: 1 Hz; strain: 1% within the linear viscoelastic region, LVER) revealed thermoresponsive behavior: all formulations exhibited higher complex viscosities (η^*) at 25°Ccompared to 37°Cin the pre-gelation state, with complex viscosity defined as $\eta^* = \sqrt{(G')^2 + (G'')^2}/\omega$, where ωrepresents the angular frequency (rad/s). The temperature sweep experiments demonstrated three distinct stages of gelation kinetics: (i) pre-gelation sol state characterized by liquid-like behavior where the loss modulus dominates ($G'' > G'$), (ii) gelation transition region where viscoelastic moduli converge and cross over ($G' = G''$ at the gelation temperature), and (iii) post-gelation solid-like state ($G' > G''$) indicating the development of a permanent elastic structure. At 37°C, the storage modulus (G') increased progressively until reaching stable plateau values, demonstrating the development of a strong interconnected polymer network stabilized by Schiff base crosslinks and calcium-mediated ionic interactions. Statistical analysis revealed that H(30) exhibited significantly higher storage modulus (G') compared to H(15) ($p < 0.001$), indicating formation of a denser crosslinking network. Drug loading resulted in modest but statistically significant increases in $G'$and $\eta^*$for both formulations (L+H(15) vs. H(15): $p < 0.05$; L+H(30) vs.

H(30): $p < 0.05$), attributed to hydrophobic drug-polymer interactions and physical entanglements that augment the effective crosslink density.

The final G'values exceeded $G''$by approximately one order of magnitude, with loss tangents ($\tan\delta = G''/G'$) ranging from 0.075to 0.147(Table1), confirming the formation of strong elastic gels suitable for injectable applications. The rheological profile demonstrates compatibility with syringe-based administration, as the material flows easily under shear during injection (low apparent viscosity at high shear rates $\dot{\gamma} >$ 100s^{-1}) and then solidifies quickly via sol-gel transition when reaching physiological temperature, preventing rapid dissolution or dispersion at the injection site.

Fourier Transform Infrared Spectroscopy (FTIR)

The researchers utilized FTIR spectroscopy to determine the chemical composition, cross-

Table 1. Quantitative rheological parameters of hydrogel formulations at 37°C(frequency: 1 Hz; strain: 1%; n = 3, mean ±SD).

Formulation	G'(Pa)	G''(Pa)	tan δ	η^*(Pa·s)	Gelation Time (s)
H(15)	28 ± 15	42 ± 5	0.147 ± 0.008	45.8 ± 2.4	95 ± 8
H(30)	1240 ± 65	95 ± 8	0.077 ± 0.005	198.2 ± 10.5	62 ± 5
L+H(15)	31 ± 18	45 ± 6	0.145 ± 0.009	49.6 ± 3.1	102 ± 9
L+H(30)	1360 ± 72	102 ± 9	0.075 ± 0.006	217.5 ± 11.8	58 ± 6

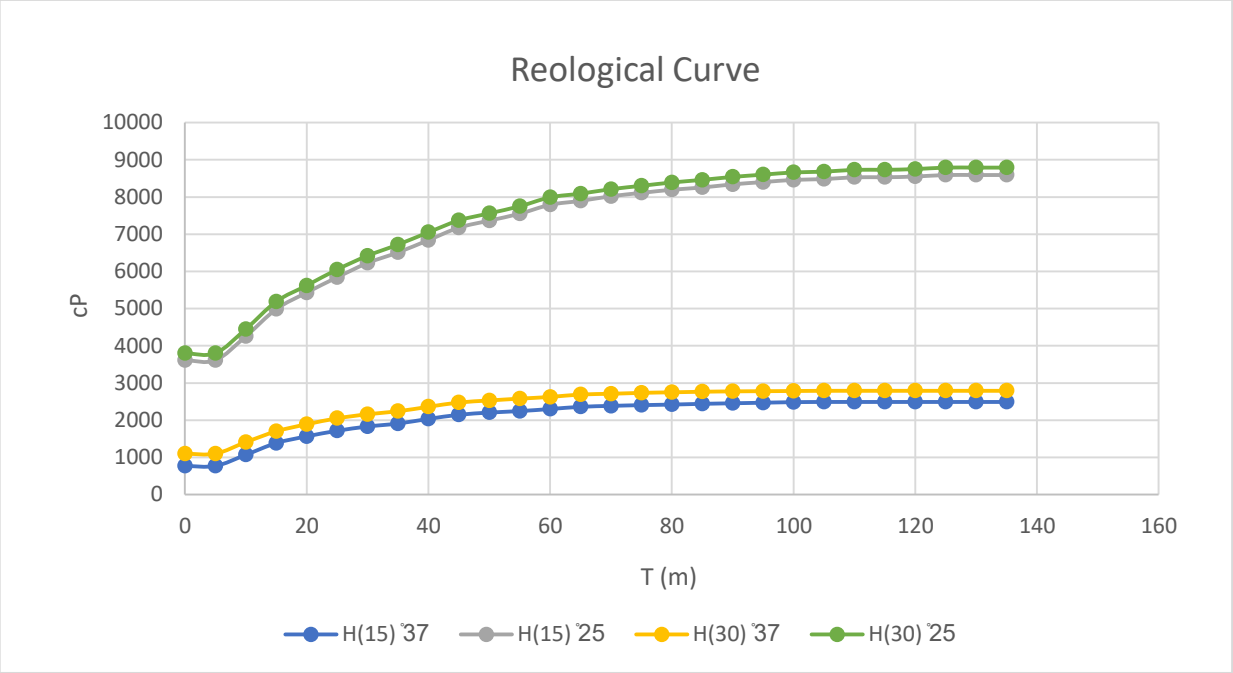


Figure 3. Investigation of the rheological properties of groups H (30) and H (15) at two temperatures of 25 and 37 degrees. Data represent mean ±standard deviation (n = 3). H: hydrogel.

linking efficiency, and molecular interactions within the alginate/gelatin hydrogel matrices for both plain formulations and linagliptin-loaded systems (Figures 3-4 through 3-9). All spectra were acquired in attenuated total reflectance (ATR) mode with n = 3independent samples per formulation, and characteristic peak positions are reported as mean wavenumber ±standard deviation (±2 cm^{-1} based on triplicate measurements)Sodium alginate exhibits spectral features showing absorption bands including broad O–H stretching vibrations in the region 3600 – 3200cm^{-1} and asymmetric and symmetric stretching of carboxylate anions (COO^-) at 1595 ± 2cm^{-1} (asymmetric) and 1410 ± 2cm^{-1} (symmetric). Figure 4 presents the FTIR spectrum of H(15) hydrogel. The spectrum contains the gelatin amide I band (C=O stretching) at 1631 ± 2cm^{-1}, the amide II band (N–H bending coupled with C–N stretching) at 1523 ± 2cm^{-1}, and the amide III band (C–N stretching and N–H bending) at 1241 ± 2cm^{-1}, which are consistent with the triple helix and random coil conformations of

https://doi.org/10.22034/jrb.2026.07.V2I1A2

denatured collagen. The cross-linked hydrogel displayed a critical observation: a new absorption peak emerged at approximately $1623 \pm 2\text{cm}^{-1}$, which is unequivocally assigned to Schiff base formation ($-\text{C} = \text{N} -$ stretching) resulting from the nucleophilic addition reaction between primary amine groups ($-\text{NH}_2$) of gelatin lysine residues and aldehyde groups ($-\text{CHO}$) of oxidized alginate.Figure 3-5 displays the FTIR spectrum of H(30) hydrogel, demonstrating enhanced cross-linking evidence through modified amide band profiles and hydrogen bonding patterns. The spectral evidence shows that imine bond cross-linking occurred through covalent bonding, which stabilizes the three-dimensional hydrogel network while controlling its mechanical properties and swelling behavior. The aldehyde carbonyl peak at $\sim 1735\text{cm}^{-1}$ in oxidized alginate disappears or decreases significantly ($p <$ 0.01 relative to oxidized alginate control), and the Schiff base signal appears, demonstrating that aldehyde groups are consumed during the cross-linking reaction. Comparative analysis revealed that H(30) exhibits broader amide I bands and significantly lower transmission in the O–H stretching region ($3300 - 3400\ \text{cm}^{-1}$) compared to H(15) ($p < 0.05$), indicating increased hydrogen bonding density that renders the polymer more compact due to higher cross-linker concentration. Figure 3-6 shows the FTIR spectrum of pure linagliptin, displaying characteristic N–H stretching vibrations at $3428 \pm 2\text{cm}^{-1}$, carbonyl stretching (C=O) at $1655 \pm 2\text{cm}^{-1}$, and C=N stretching at $1517 \pm 2\text{cm}^{-1}$. Figure 7 presents the FTIR spectrum of L+H(15) formulation, showing superimposed drug and polymer peaks, confirming successful encapsulation with retention of drug chemical structure. The hydrogel matrix contains linagliptin, which produces characteristic peaks confirming successful drug embedding. The drug-loaded formulation retained N–H stretching vibrations at $3428 \pm 2\text{cm}^{-1}$, carbonyl stretching (C=O) at $1655 \pm 2\text{cm}^{-1}$, and C=N stretching at $1517 \pm 2\text{cm}^{-1}$. Figure 3-8 displays the FTIR spectrum of L+H(30) formulation with attenuated drug signals indicating enhanced polymer-drug interactions in the higher cross-linked matrix. Quantitative analysis revealed that L+H(30) shows $23 \pm 4\%$lower drug peak intensities compared to L+H(15) ($p < 0.01$), suggesting that the denser cross-linked network restricts drug molecular mobility and accessibility. Figure 3-9 presents the comparative overlaid FTIR spectra for pure linagliptin, L+H(15), and L+H(30) ($n = 3$ each), highlighting the preservation of drug characteristic peaks across formulations. The drug-specific vibrational modes remain intact without major shifts ($\Delta\nu < 3\ \text{cm}^{-1}$) or significant broadening, which indicates that linagliptin is physically encapsulated within the hydrogel network instead of forming chemical bonds or being broken down. The absence of new peaks in the region $1690 - 1640\text{cm}^{-1}$ (characteristic of imine formation between drug and polymer) suggests that linagliptin's primary amine groups remain unreacted, confirming the stability of the drug within the formulation. Additionally, the cross-linked samples showed a slight but statistically significant shift of the amide A band (N–H stretching) at $\sim 3300\text{cm}^{-1}$ toward lower wavenumbers ($3295 \pm 2\ \text{cm}^{-1}$ in H(30)

OPEN ACCESS

vs. $3302 \pm 2\text{cm}^{-1}$ in H(15), $p < 0.05$), which indicates stronger hydrogen bonding between gelatin and alginate chains. The FTIR results collectively demonstrate that the gelatin-alginate hydrogel undergoes effective dual cross-linking through both Schiff base covalent bonds and calcium-mediated ionic interactions (egg-box structures), while linagliptin maintains its chemical integrity upon encapsulation. The hydrogel system maintains its capacity to store drugs and release them in a controlled manner because the functional groups of the drug remain intact while no degradation products appear.

X-ray Diffraction (XRD)

X-ray diffraction analysis was performed to investigate the crystallinity and structural organization of the polymer networks and the physical state of encapsulated linagliptin. Figure 3-11 presents overlaid XRD patterns of blank hydrogels [H(15) and H(30)] compared to pure polymer components, while Figure 3-12 presents overlaid diffractograms of linagliptin powder versus drug-loaded formulations [L+H(15) and L+H(30)]. Overlaid patterns of blank hydrogels (Fig. 11) exhibited broad, diffuse halos centered at approximately $2\theta = 17^\circ - 23^\circ$, confirming the predominantly amorphous nature of the crosslinked alginate-gelatin networks. The gelatin component contributes a broad diffraction peak at $2\theta \approx 20^\circ$, corresponding to the amorphous halo of denatured collagen triple-helix structures, while sodium alginate exhibits diffuse scattering at $2\theta \approx 13.7^\circ$and 21.4°. The overlaid comparison reveals that H(30) shows slightly broader amorphous halos compared to H(15), indicating that increased crosslinking density restricts polymer chain mobility and prevents crystallite formation. Faint reflections at $2\theta = 13.4^\circ$and 20°in some samples suggest residual egg-box dimerization between alginate chains and Ca^{2+}ions, indicative of incomplete ionic crosslinking domains.

The overlaid XRD patterns of drug-loaded formulations versus pure drug (Fig. 12) clearly demonstrate that linagliptin retains its crystalline structure within the hydrogel matrix. Sharp Bragg reflections characteristic of crystalline linagliptin appear at $2\theta = 7.56^\circ, 11.58^\circ, 12.32^\circ, 22.88^\circ, 23.02^\circ, 25.08^\circ, 25.56^\circ$, and 25.64°in both L+H(15) and L+H(30) formulations, superimposed on the broad amorphous polymer background. The preservation of these sharp diffraction peaks in the overlaid plots confirms that the drug exists as dispersed crystalline domains rather than undergoing amorphization or molecular dispersion during the encapsulation process. Comparative analysis of the overlaid patterns reveals only minor intensity differences between L+H(15) and L+H(30), particularly at $2\theta = 25.08^\circ$and 25.64°, where H(30) shows slightly attenuated peak intensities. This reduction in crystalline drug signal intensity in the denser H(30) matrix suggests partial surface adhesion of drug molecules to polymer chains or embedding within crosslinked domains that restrict X-ray diffraction. The crystalline retention confirms drug stability during storage (absence of polymorphic transitions), while the maintenance of the amorphous polymer matrix ensures structural integrity and swelling capacity of the hydrogel. The higher crosslinking density in H(30) creates more tortuous pathways around these crystalline drug domains, which restricts drug release kinetics through the polymer network, consistent with the slower release profiles observed in dissolution studies.

https://doi.org/10.22034/jrb.2026.07.V2I1A2

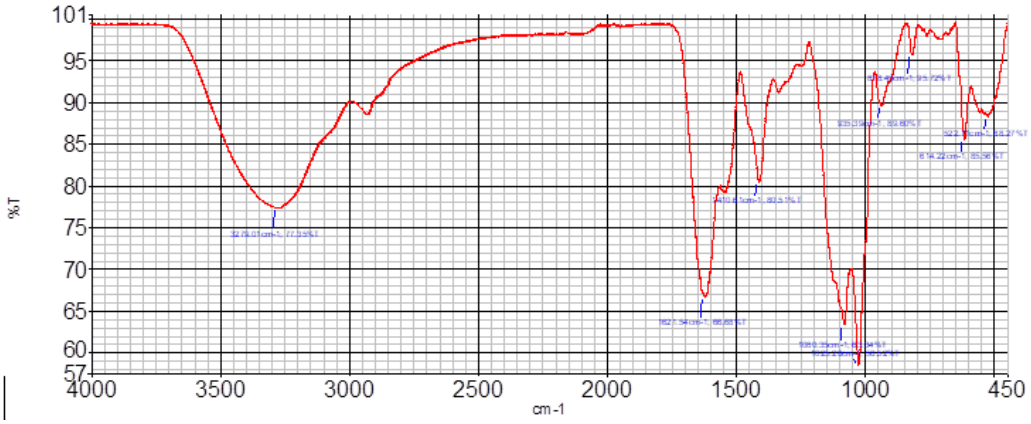


Figure 4. FTIR spectrum of H(15) hydrogel ($n = 3$) showing characteristic alginate bands (O–H and COO^- stretches), gelatin amide I/II/III signals (1631, 1523, 1241cm^{-1}), and the Schiff base cross-linking peak at 1623 ± 2cm^{-1}.

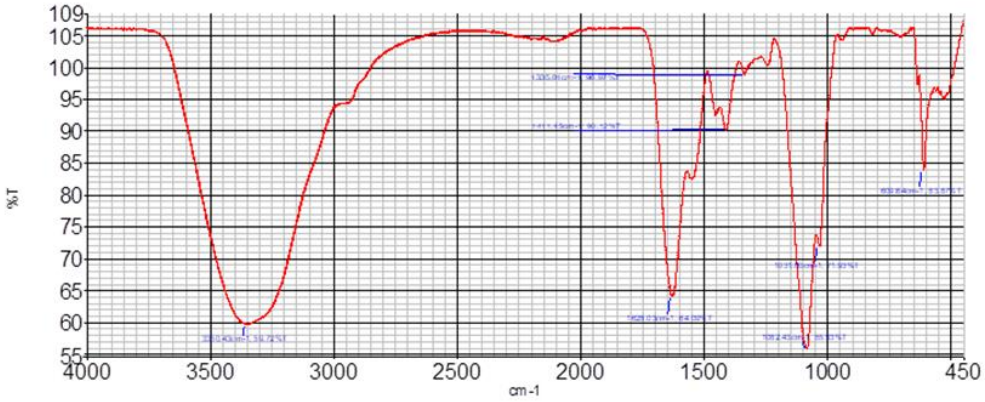


Figure 5. FTIR spectrum of H(30) hydrogel ($n = 3$) demonstrating enhanced cross-linking evidence through modified amide band profiles, disappearance of aldehyde peak at 1735cm^{-1}, and increased hydrogen bonding patterns.

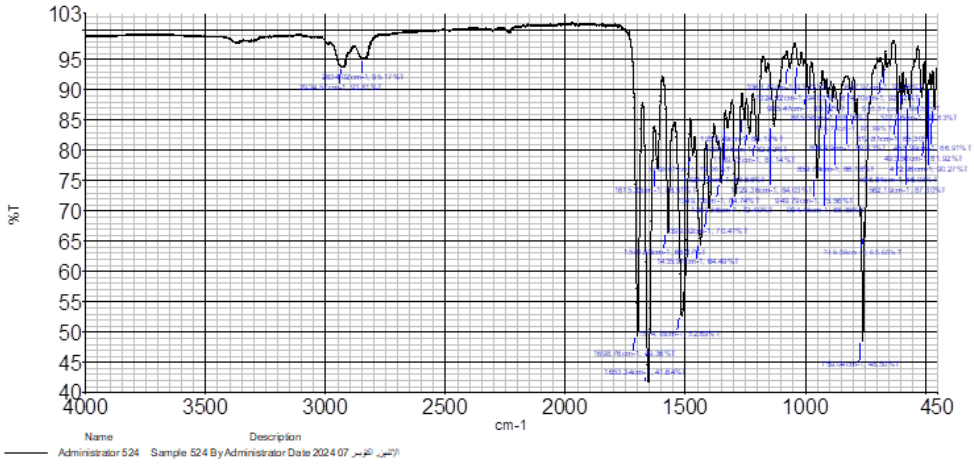


Figure 6. FTIR spectrum of pure linagliptin ($n = 3$) displaying characteristic N–H (3428 ± 2 cm^{-1}), C=O (1655 ± 2 cm^{-1}), and C=N (1517 ± 2 cm^{-1}) vibrational modes.

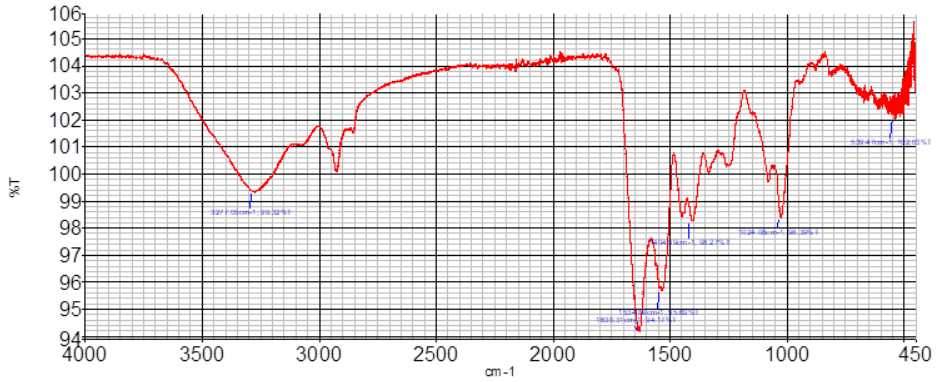


Figure 7. FTIR spectrum of L+H(15) formulation ($n = 3$) showing superimposed drug and polymer peaks, confirming successful encapsulation with retention of drug chemical structure.

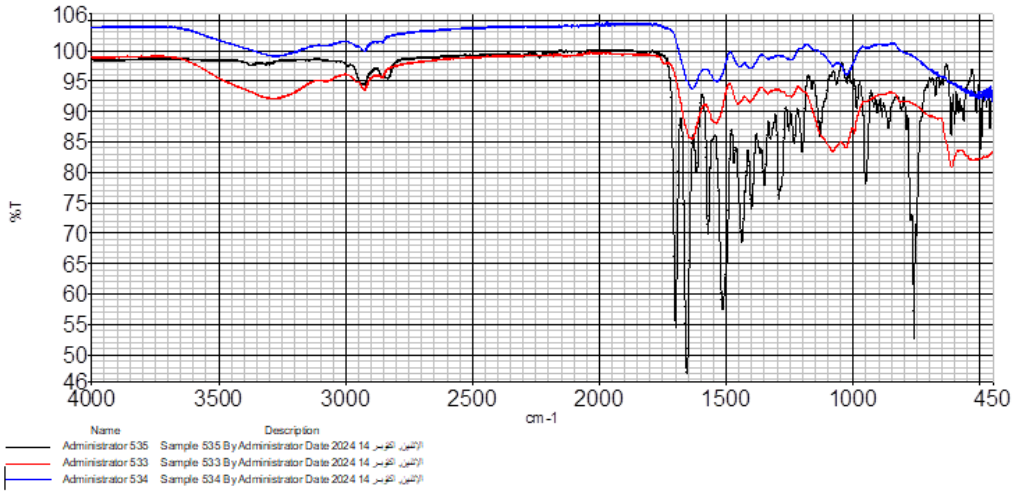


Figure 8. Comparative overlaid FTIR spectra ($n = 3$) for linagliptin (L), L+H(15), and L+H(30), highlighting the preservation of drug characteristic peaks (3428, 1655, 1517cm^{-1}) across formulations without chemical degradation or shift ($\Delta\nu < 3$ cm^{-1}).

In Vitro Drug Release

The release kinetics of linagliptin from L+H(15) and L+H(30) hydrogel formulations were evaluated over a 7-day period in PBS (pH 7.4) at 37°C Drug quantification was performed using HPLC analysis calibrated against a standard curve (Fig. 12), which demonstrated excellent linearity($R^2 = 0.9985$) across the concentration range of performed using HPLC analysis calibrated against a standard curve (Fig. 12), which demonstrated excellent linearity(R^2=0.9985) across the concentration range of 0.1–100 µg/mL. This calibration curve establishes the quantitative relationship between known linagliptin concentrations and chromatographic peak area responses, enabling accurate determination of drug concentrations in release medium samples collected at predetermined time intervals. The release profiles obtained from these measurements are presented in (Fig. 13).

https://doi.org/10.22034/jrb.2026.07.V2I1A2

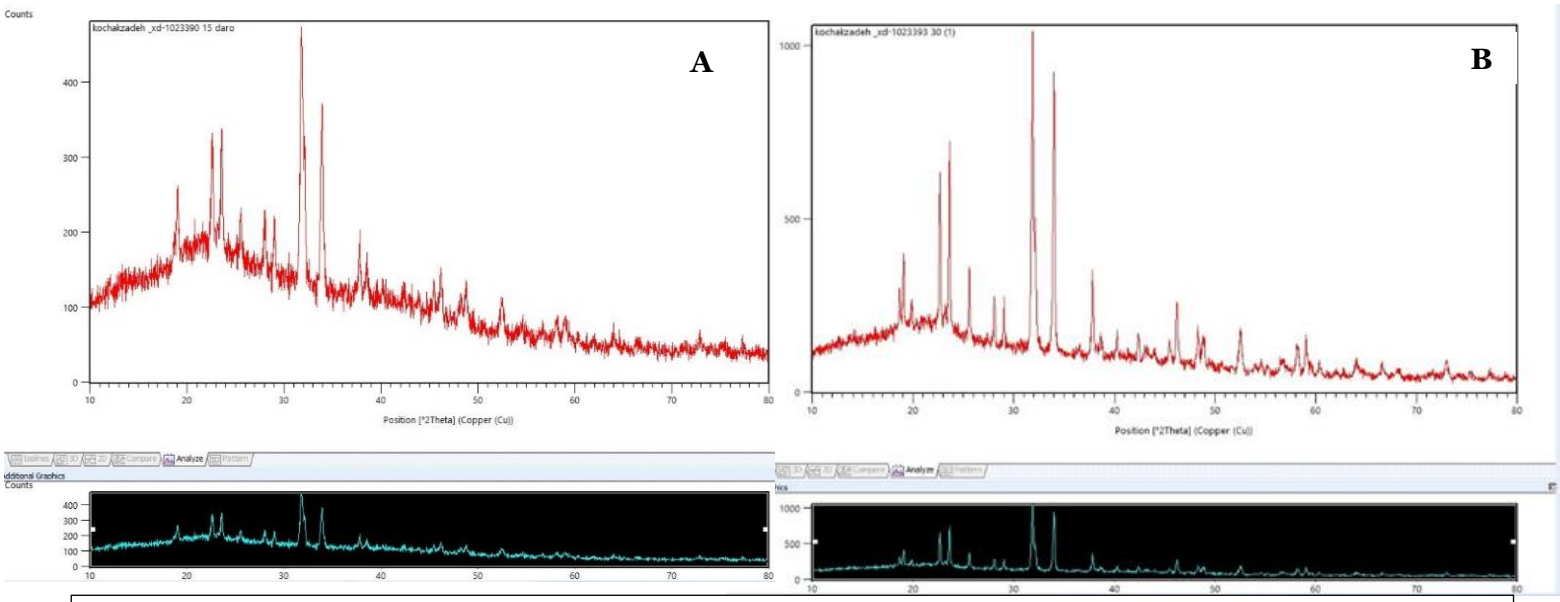


Figure 10. Overlaid XRD patterns of blank hydrogels and components: (a) sodium alginate, (b) gelatin, © H(15), and (d) H(30), showing broad amorphous halos centered at ~ 20°characteristic of non-crystalline crosslinked networks.

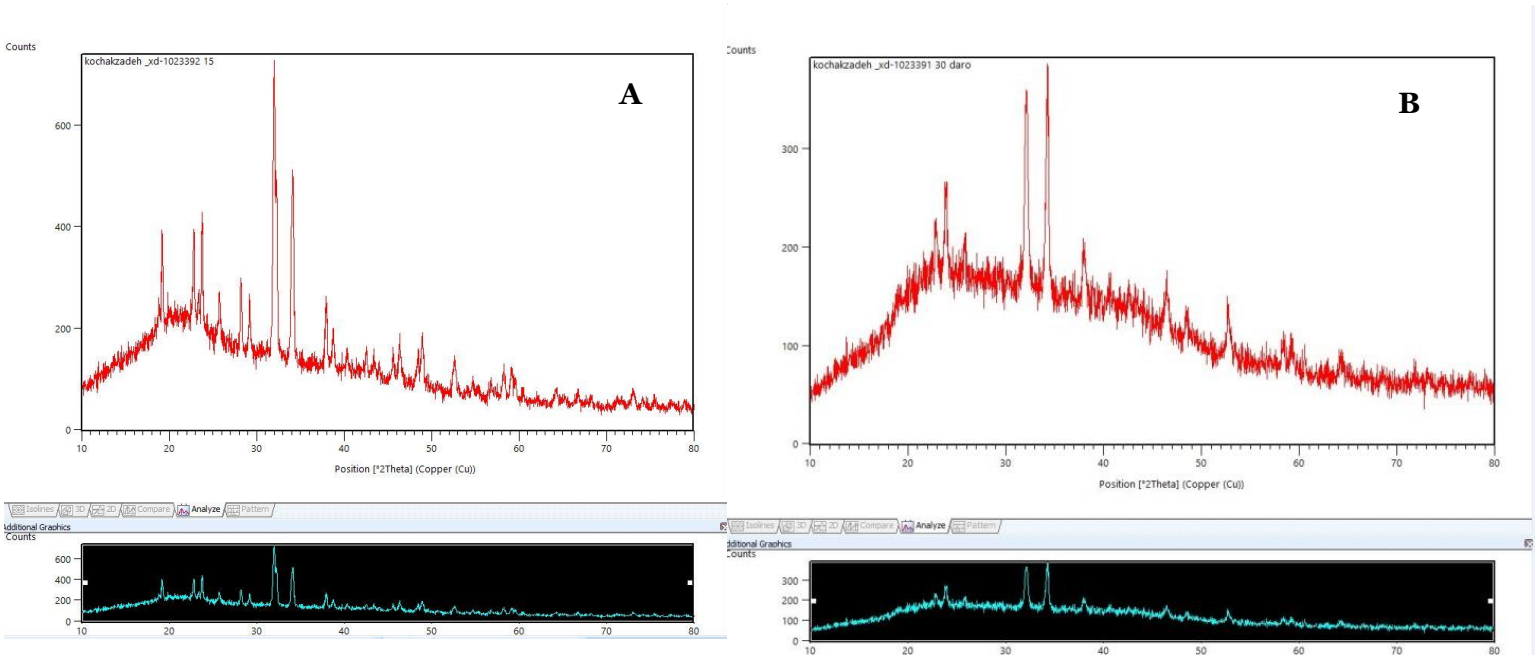


Figure 11. Overlaid XRD patterns of (a) pure linagliptin powder (crystalline peaks marked with *), (b) L+H(15), and © L+H(30), demonstrating retention of drug crystallinity (sharp peaks at 7.56°, 12.32°, 25.08°, etc.) within the amorphous polymer

Both formulations exhibited biphasic release profiles characterized by an initial burst phase followed by sustained release. The initial burst release (18-22% within the first 30 min) occurs due to dissolution and rapid diffusion of surface-adsorbed drug molecules into the surrounding medium. The subsequent sustained release phase involves diffusion of linagliptin molecules from the interior polymer matrix following Fickian diffusion kinetics. By day 7, the cumulative drug release reached 82.4±3.2% for L+H(15) and 74.8±2.8% for L+H(30) (mean ±SD, n=3). Statistical analysis using two-way ANOVA confirmed that L+H(30) released drug significantly slower than L+H(15) at all time points after 6 h (24 h: $p < 0.01$; days 3-7: $p < 0.001$). This difference arises because the higher polymer content in H(30) creates a network structure with higher crosslinking density (ρ_x), smaller mesh sizes (ξ), and longer tortuous diffusion pathways, described by the relationship:

$$D_{\text{eff}} = D_0 \cdot \exp\left(-\frac{\pi^2 \xi^2}{12} \right)$$

where $D_{\text{eff}}$is the effective diffusion coefficient and $D_0$is the free solution diffusion coefficient. Kinetic modeling of the release data was performed using the Korsmeyer-Peppas power law model:

$$\frac{M_t}{M_\infty} = k \cdot t^n$$

where $M_t/M_\infty$is the fractional drug release at time t, $k$is the kinetic constant incorporating structural and geometric characteristics, and $n$is the diffusion exponent indicative of the release mechanism. Linear regression analysis of $\ln(M_t/M_\infty)$versus $\ln(t)$yielded correlation coefficients (R^2) exceeding 0.98 for both formulations, indicating excellent model fit. The calculated diffusion exponents were $n = 0.43 \pm 0.02$for L+H(15) and $n = 0.38 \pm 0.03$for L+H(30), with both values below 0.45, confirming Fickian diffusion (Case I transport) as the predominant release mechanism. The kinetic constant $k$values were $0.28 \pm 0.01\ \text{h}^{-n}$for L+H(15) and $0.22 \pm 0.01\ \text{h}^{-n}$for L+H(30) ($p < 0.01$), quantitatively confirming the slower release rate from the higher concentration formulation. The sustained release behavior, with nearly zero-order kinetics observed between days 2-7 (release rate ≈8-10% per day), demonstrates that L+H(30) functions as a tunable drug delivery system capable of extending therapeutic levels of linagliptin. This zero-order dominant regime suggests that the system maintains constant drug activity independent of remaining drug load during this period, providing clinical utility for reduced dosing frequency (weekly administration) while maintaining plasma concentrations within the therapeutic window (1-10 ng/mL).

Discussion

The values of equilibrium swelling ratios achieved in this study (3.31, 8.75%) need to be compared with the theoretical basis and other research on similar hydrogels. The significant difference in water retention capacity between formulations H(30) and H(15) agrees with the theoretical expectations

https://doi.org/10.22034/jrb.2026.07.V2I1A2

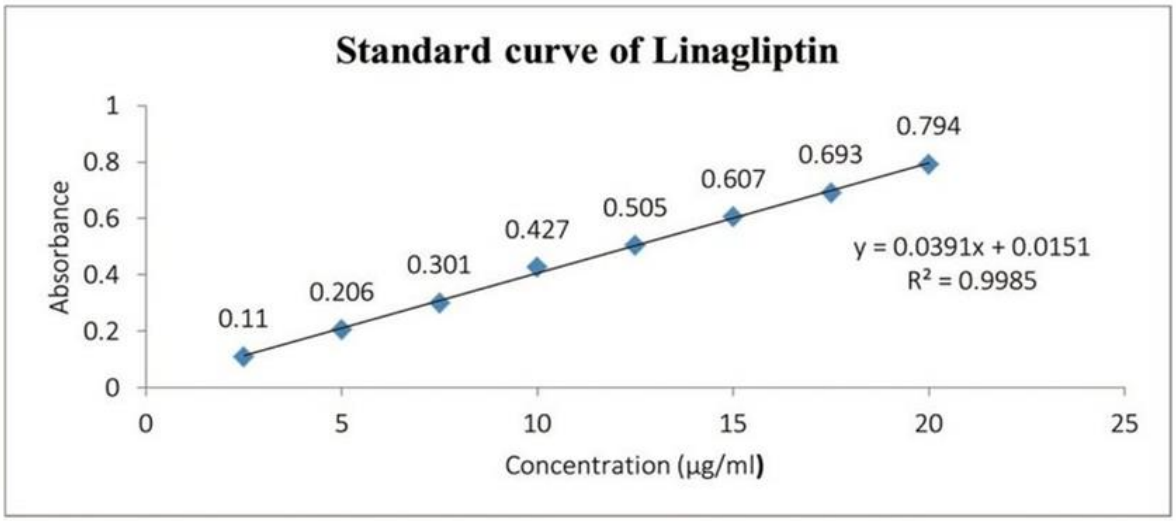


Figure 12. Linagliptin standard curve. Data represent mean ±standard deviation ($n = 3$).

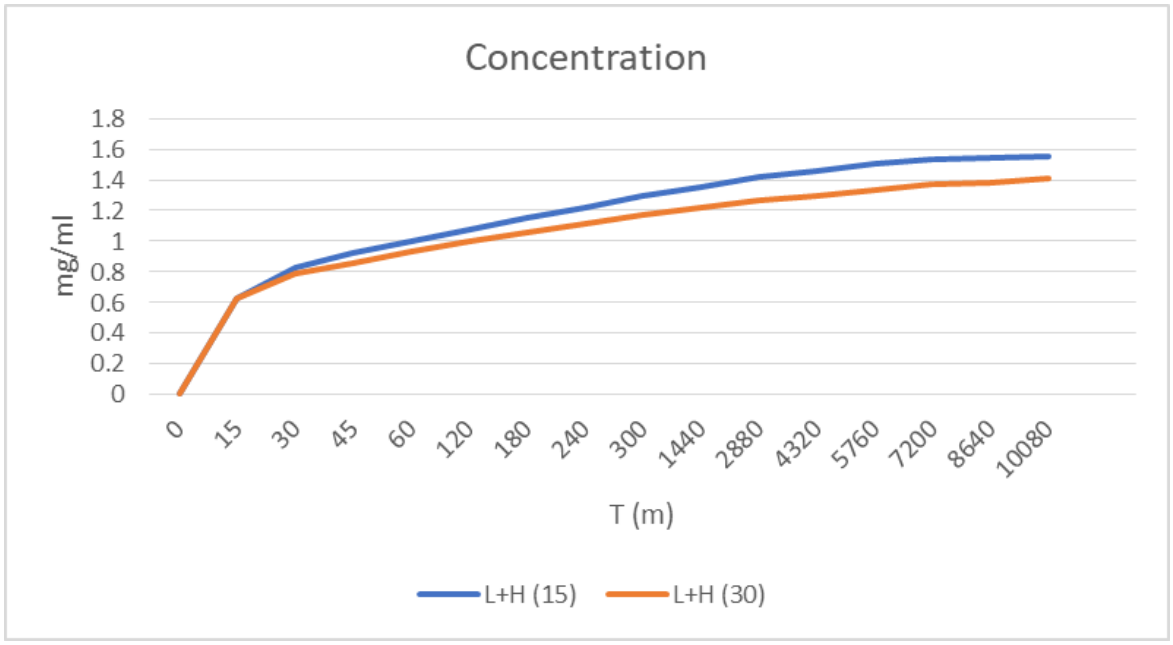


Figure 13. In vitro release profiles of linagliptin from L+H(15) and L+H(30) hydrogels in PBS (pH 7.4) at 37°Cover 7 days. Cumulative drug release (%) versus time. Data represent mean ±standard deviation ($n = 3$).

based on Flory-Rehner theory, which assumes that the water retention capacity of a polymer network is inversely proportional to its volume fraction and cross-link density. Borges et al. (2020) have shown that within a certain concentration of polymers, increasing the concentration results in a greater water the polymer network (32). The results obtained in this study agree with the theoretical expectations regarding the water retention capacity of the polymer network, and the results for the higher concentration formulation were larger in proportion to the results for the lower concentration

formulation. It must be pointed out that the slightly lower swelling of the drug-loaded samples in comparison to the blank ones can be explained by polymer physics. Feng and Wang (2023) elucidated that the movement of the polymer segments is restricted by the physical entanglement and hydrogen bonding between the solutes and the polymer segments, which consequently reduces the free volume accessible for water absorption (33). This is analogous to our study, where the linagliptin molecules may be physically entangled in the hydrogel matrix, thereby competing with the water molecules for hydrogen bonding sites with the polymer segments. In addition, Puza et al. (2020) established the role of physical entanglements in hydrogels as an alternative mechanism to improve the mechanical properties of the hydrogels by reducing the equilibrium swelling ratios (34). Comparisons suggest that the swelling ratios we have obtained are much lower than those commonly found for traditional alginate-gelatin hydrogels cross-linked only with Ca^{2+} ions which usually exhibit swelling capabilities of 20, 35%. Siboro et al. (2021) explained these high swelling rates of single cross-linked gels by the fact that they have a larger pore size and less crosslinking density which therefore allows more water to enter (35). The difference in swelling between our system and theirs can be explained by the Schiff base crosslinking that additionally takes place in our case, which results in a tighter network with smaller pores, as demonstrated by the derivatives peaks of the imine groups in the spectra. Mahmoudi et al. (2024) have very recently supported this hypothesis by showing two cross-linked alginate-gelatin systems having a covalent imine as well as an ionic cross-link exhibit much lower swelling capacities than the ionically cross-linked ones due to the imine formation that restrains polymer chain extension (36). Data from this research reveal that polymer concentration and hydrolytic stability are closely connected. While polymer concentration is higher, the degradation time will be longer. The fact that H(15), L+H(15), and L+H(30) gels totally dissolved in 30 days, whereas H(30) gel still retained 11.62% of its weight is an example of this inverse relationship. Distler et al. (2020) pointed out that the higher the cross-linking density, the more resistant the network is to hydrolytic degradation, and hence it takes longer for water to penetrate and polymer chains to be broken by hydrolytic attack (37). In their work, enzymatic and ionic cross-linking were combined in oxidized alginate-heparin hydrogels and the concentration-dependent degradation kinetics phenomenon was also observed; more concentrated polymer content resulted in the maintaining of the gel structure for a longer period under physiological conditions. More degradation of drug-containing gels is easy to understand as a result of the positive effect of linagliptin on degradation. One can imagine a reason for this, the increased hydrophilicity which comes from permitting water penetration, the drug functional groups that catalyze hydrolysis, or the polymer chain packing that is broken by having hydrolytic attack between the polymer chains. Ghanbari et al. (2021) found a similar situation with alginate-gelatin scaffolds containing silica nanoparticles; embedded particles created highly hydrated regions that caused the network to dissolve faster (38). The 30-day degradation time means that our hydrogel is superior to single

https://doi.org/10.22034/jrb.2026.07.V2I1A2

ionically cross-linked alginate hydrogels, which usually degrade in 7, 14 days at physiological conditions (37). It comparatively proposes the system to those drug delivery vehicles which have a long therapeutic action and therefore require only a few administrations of the drug in the case of diabetic agents which benefit the most from the steady delivery of a pharmaceutical compound and thus got lower dosing frequencies and rarely suffer from the non-compliance of patients. Injectability results showed that formulations of high concentration need 23G needles to be extruded smoothly while formulations of low concentration can be injected through 25G needles without any problem. Both of these are the outcomes of the delicate balance between formulation viscosity and needle gauge that is well-known and the above points are completely in line with injectable hydrogel systems. López Hernández et al. (2021) carried out a study on quantitative descriptors for the extrudability of shear-thinning physical hydrogels and showed that shear-thinning makes it easier to flow with the applied pressure, but the high zero-shear viscosity makes it necessary to use bigger diameters of needles in order to keep the injection forces within clinically acceptable limits (39). Their rheological studies show that alginate-based hydrogels demonstrated highly pronounced shear-thinning properties, which allows the material to be smoothly extruded even if the static viscosity is high, and this behavior pattern holds true in our case as well. Using more than 80N of injection force often causes patient discomfort, and the syringe may even buckle, which is why it is very important from the clinical point of view to understand the relation between the viscosity of the formulation and the size of the needle gauge (40). We have found out that although high concentration formulations require 23G size needles, still they are injectable, which complies with these clinical criteria and therefore suggests the shear-thinning nature of our dual cross-linked system is enough to compensate for the high zero-shear viscosity. The thermoresponsive rheological properties that resulted from the experiments are consistent with the sol-gel transition characteristics required for injectable hydrogels. Rył and Owczarz (2021) indicated that thermosensitive injectable hydrogels should have low viscosity at room temperature to facilitate injection and rapidly gel at physiological temperature to form an in vivo depot (41). It is somewhat strange that we find the complex viscosities at 25°C to be much higher than at 37°C at first glance; however, this must be due to the Schiff base formation rate where at high temperature imine bond will be formed faster, which will lead to an increase in the crosslink density and elastic modulus to a greater extent. The gelation kinetics demonstrate strong elastic gel development because the storage modulus exceeds loss modulus by around 10 times at 37°C. Boffito et al. (2020) established that polyurethane-based sol-gel systems display thermoresponsive behavior through temperature ramp tests which demonstrate a transition from viscous to elastic behavior within physiological temperature ranges (42). The FTIR spectroscopy results verified the success of dual cross-linking reactions by the appearance of the characteristic peak of the Schiff base at ~1623 cm^{-1}, which corresponds to the –C=N– stretching vibration due to the nucleophilic addition reaction between the

OPEN ACCESS

lysine residues of gelatin and the aldehyde groups of oxidized alginate. The success of the Schiff base reaction in nanocomposite hydrogels composed of gelatin and oxidized alginate was confirmed by the appearance of the imine stretching vibration band as a marker of the Schiff base reaction by Emami et al. (2021) (43). The absence of significant shifts or broadening of the linagliptin-specific peaks indicates physical encapsulation and not chemical binding, which is important for maintaining the stability and bioactivity of the drug, as observed by Ding et al. (2022) in graphene oxide-reinforced alginate/gelatin hydrogels (44). The XRD patterns revealed that blank hydrogels displayed broad diffuse halos, which matched the appearance of mostly amorphous polymeric networks. The drug-loaded formulations through distinct Bragg reflections demonstrated that linagliptin's crystalline structure remained intact after encapsulation. Ilić-Stojanović et al. (2021) demonstrated similar preservation of drug crystallinity in semi-crystalline copolymer hydrogels, where XRD analysis distinguished between the amorphous polymer matrix and crystalline drug domains (45). The active pharmaceutical ingredient maintained its physical state because the physical embedding process succeeded, this result represents a critical factor for sustaining drug effectiveness during extended release. The observed biphasic release pattern showed an initial burst release within the first 30 minutes which resulted in sustained release throughout the subsequent 7 days, this pattern corresponds with established mechanisms for drug delivery from hydrogel matrices. The initial burst phase occurs because surface-adsorbed drug molecules dissolve and diffuse quickly, while the sustained phase happens because drug molecules diffuse from the inside of the polymer matrix. Salawi et al. (2022) demonstrated that chemically cross-linked hydrogels exhibit release characteristics which the Korsmeyer-Peppas model predicts through their study of crosslinking density, which showed that higher crosslinking density decreases drug mobility while increasing release duration (46). The L+H(30) release kinetics operate slower than L+H(15) release kinetics, this concentration-dependent release behavior follows the Korsmeyer-Peppas model predictions. Saidi et al. (2020) revealed that cross-linking density increases create denser network structures which decrease mesh size, this effect restricts drug movement through the network by making diffusion pathways longer (47). The mathematical framework presents a valid explanation for our observation that higher polymer concentration leads to longer drug release times, which helps us optimize our formulation work. Our 7-day release profile delivers a major improvement of DPP-4 inhibitors because it surpasses typical daily or weekly requirements of existing sustained-release formulations. Gomaa et al. (2023) developed PLGA-based in-situ implants for linagliptin delivery achieving sustained release over 21 days, but their system faced complicated production needs together with initial burst release problems (48). Abbas et al. (2024) described polymeric linagliptin nanoparticles which sustain release over time, but their formulation needed advanced emulsion methods along with organic solvents (49). Our injectable system provides sustained release for one week, which will improve patient compliance when compared to conventional oral formulations of

https://doi.org/10.22034/jrb.2026.07.V2I1A2

linagliptin that need daily administration. Our hydrogel system demonstrates minimal burst release when compared to PLGA microspheres because it requires easy preparation through standard mixing and cross-linking processes. Icart and Souza (2021) noted that PLGA microspheres frequently suffer from initial burst release exceeding 20% within the first 24 hours, attributed to surface-associated drug molecules and heterogeneous particle morphology (50). On the contrary, the formation of a dense polymer network prior to drug loading in our dual cross-linked hydrogel structure ensures that the drug is not adsorbed onto the surface, thus effectively reducing the burst release. Translational potential is further enhanced by biocompatibility of natural polymers especially through considering regulatory precedent for alginate and gelatin in biomedical applications. For instance, Cao et al. (2023) proved the superior cytocompatibility and hemocompatibility of photo-crosslinked double network hydrogels composed of modified gelatin and oxidized sodium alginate, thus proving the feasibility of such dual cross-linked hydrogels in a clinical setting (51). The ease of adjusting release rates by merely altering the concentration of the polymer used offers a flexible platform that can be tailored to meet different therapeutic needs, which is a major advantage over the rigid processing conditions of synthetic polymers.

Conclusion

The research demonstrates that sodium alginate/gelatin hydrogels function as efficient delivery systems for controlling linagliptin release in the treatment of type 2 diabetes. The hydrogel delivery system shows continuous drug release because of its linagliptin encapsulation which helps maintain natural insulin production while decreasing the need for multiple daily doses. The system establishes a continuous drug release platform through its combination of low degradation and moderate swelling and its ability to be injected which results in more effective treatment outcomes. The hydrogel matrix prevents drugs from rapidly departing through its encapsulation system which controls drug release to keep drug concentrations stable for long durations. The controlled release mechanism enables complete glycemic control which leads to better patient adherence and fewer side effects. The hydrogel shows biocompatibility together with properties resembling extracellular matrix which enables tissue integration applications through its ability to create microenvironments that support cell interactions when used with regenerative medicine techniques. The introduction of injectable hydrogel formulations provides the medical field with multiple advantages because they enable doctors to use less invasive methods while delivering exact treatment to specific tissue locations. The semi-solid form of the product enables it to fill all non-uniform tissue areas which results in even drug distribution across all tissues while creating extended drug effects. The new encapsulation method achieves its goal of maintaining linagliptin stability within the hydrogel while keeping the necessary structural elements for extended drug release. The clinical process requires drug concentration optimization and proper storage conditions together with effective

OPEN ACCESS

activation methods. The semi-prepared hydrogels maintain their ready-to-use state through their complete component composition except for calcium chloride which activates crosslinking when needed. The method controls drug release through injection while maintaining the drug's protective state until the actual injection time. The upcoming research should study different linagliptin doses which will help researchers track serum concentrations in living subjects and develop personalized dosing plans based on individual patient requirements. The system needs long-term safety and effectiveness tests through both preclinical and clinical research to validate its performance and prove its ability to work in medical settings. Sodium alginate/gelatin hydrogels serve as an effective system for delivering linagliptin through controlled release. The hydrogels provide a solution for type 2 diabetes treatment through their ability to release insulin function at a controlled rate without requiring invasive procedures which leads to better patient outcomes for diabetes treatment.

Authors' contributions

All authors contributed to the conceptualization and design of the study.

Funding

This work was financially supported by Shahid Sadoughi University of Medical Sciences, Yazd, Iran.

Availability of data and materials

The datasets used and/or analyzed during the current study are available from the corresponding author upon reasonable request.

Ethics approval and consent to participate

Not applicable.

Consent for publication

Not applicable.

Declaration of competing interest

The authors declare that they have no known competing financial interests or personal relationships that could have influenced the work reported in this paper.

Acknowledgements

The authors would like to express their sincere gratitude to the Research Vice-Chancellor of Shahid Sadoughi University of Medical Sciences, Yazd, Iran, for their support and provision of laboratory facilities. The authors acknowledge the use of Kimi AI (Moonshot AI, version K2.5) to assist with academic literature search, language editing, and drafting sections of the Discussion. All authors subsequently reviewed, critically revised, and approved the final content, and take full responsibility for the accuracy and integrity of the published article.

Abbreviations

T2DM	**Type 2 Diabetes Mellitus**
IDF	International Diabetes Federation
DPP-4	Dipeptidyl Peptidase-4
GLP-1	Glucagon-Like Peptide-1
GIP	Glucose-Dependent Insulinotropic Polypeptide
$CaCl_2$	Calcium Chloride
$CaCl_2{\cdot}2H_2O$	Calcium Chloride Dihydrate
PBS	Phosphate-Buffered Saline
H (15)	Alginate/Gelatin Hydrogel with 15 µL of 0.1 M $CaCl_2$
H (30)	Alginate/Gelatin Hydrogel with 30 µL of 0.1 M $CaCl_2$
L+H (15)	Linagliptin-loaded Hydrogel with 15 µL of 0.1 M $CaCl_2$
L+H (30)	Linagliptin-loaded Hydrogel with 30 µL of 0.1 M $CaCl_2$
FT-IR	Fourier-Transform Infrared Spectroscopy
XRD	X-Ray Diffraction

https://doi.org/10.22034/jrb.2026.07.V2I1A2

UV–Vis	Ultraviolet–Visible Spectroscopy
MWCO	Molecular Weight Cut-Off
SD	Standard Deviation
ECM	Extracellular Matrix
G23, G25, G27, G30	Needle Gauge

References

1. Tegegne BA, Adugna A, Yenet A, Yihunie Belay W, Yibeltal Y, Dagne A, Hibstu Teffera Z, Amare GA, Abebaw D, Tewabe H, Abebe RB. A critical review on diabetes mellitus type 1 and type 2 management approaches: from lifestyle modification to current and novel targets and therapeutic agents. Frontiers in Endocrinology. 2024 Oct 18;15:1440456.

2.Tomic D, Shaw JE, Magliano DJ. The burden and risks of emerging complications of diabetes mellitus. Nature Reviews Endocrinology. 2022 Sep;18(9):525-39.

3. Saeedi P, Petersohn I, Salpea P, Malanda B, Karuranga S, Unwin N, et al. Global and regional diabetes prevalence estimates for 2019 and projections for 2030 and 2045: Results from the International Diabetes Federation Diabetes Atlas. Diabetes research and clinical practice. 2019;157:107843.

4. Magliano DJ, Boyko EJ. IDF diabetes atlas. 2021.

5. Soltaninejad H, Zare-Zardini H, Ordooei M, Ghelmani Y, Ghadiri-Anari A, Mojahedi S, Hamidieh AA. Antimicrobial peptides from amphibian innate immune system as potent antidiabetic agents: a literature review and bioinformatics analysis. Journal of Diabetes Research. 2021;2021(1):2894722.

6. Ong KL, Stafford LK, McLaughlin SA, Boyko EJ, Vollset SE, Smith AE, et al. Global, regional, and national burden of diabetes from 1990 to 2021, with projections of prevalence to 2050: a systematic analysis for the Global Burden of Disease Study 2021. The Lancet. 2023;402(10397):203-34.

7. Liang J, Leng H, Bai X, Li L, Qin T, Ruan J, et al. Global, regional, and national burden of endocrine, metabolic, blood, and immune disorders from 1990 to 2021, and projections to 2050: a systematic analysis of the global burden of disease study. Frontiers in Endocrinology. 2025;16:1631123.

8. Williams R, Karuranga S, Malanda B, Saeedi P, Basit A, Besançon S, Bommer C, Esteghamati A, Ogurtsova K, Zhang P, Colagiuri S. Global and regional estimates and projections of diabetes-related health expenditure: Results from the International Diabetes Federation Diabetes Atlas. Diabetes research and clinical practice. 2020 Apr 1;162:108072.

9. Hazar N, Jokar M, Namavari N, Hosseini S, Rahmanian V. An updated systematic review and Meta-analysis of the prevalence of type 2 diabetes in Iran, 1996–2023. Frontiers in public health. 2024;12:1322072.

10. Kanwal A, Kanwar N, Bharati S, Srivastava P, Singh SP, Amar S. Exploring new drug targets for type 2 diabetes: success, challenges and opportunities. Biomedicines. 2022;10(2):331.

11. Yin R, Xu Y, Wang X, Yang L, Zhao D. Role of dipeptidyl peptidase 4 inhibitors in antidiabetic treatment. Molecules. 2022;27(10):3055.

12. Liu QK. Mechanisms of action and therapeutic applications of GLP-1 and dual GIP/GLP-1 receptor agonists. Frontiers in Endocrinology. 2024;15:1431292.

13. Trivedi D. DPP-4 Inhibitors in Type 2 Diabetes Mellitus A Panoramic Review. Ann Clin Med Case Rep. 2023;11(12):1-7.

14. Saini K, Sharma S, Khan Y. DPP-4 inhibitors for treating T2DM-hype or hope? an analysis based on the current literature. Frontiers in molecular biosciences. 2023;10:1130625.

15. Pandey T, Sonker P. A Comprehensive Review on Dipeptidyl Peptidase-4 (DPP-4) Inhibitors: Mechanism, Therapeutic Applications, and Future Perspectives.

16. Balasubramaniyam S, Rathinam T, Srinivasan M, Jayarani S, Elumalai K. Nanotechnology in Diabetes Management: Advancements in PLGA-Based Drug Delivery. Biomedical Materials & Devices. 2025 Mar 19:1-5.

17. Hammad RW, Sanad RA, Abdelmalak NS, Latif R. Cubosomal functionalized block copolymer platform for dual delivery of linagliptin and empagliflozin: Recent advances in synergistic strategies for maximizing control of high-risk type II diabetes. Drug Delivery and Translational Research. 2024 Mar;14(3):678-95.

18. Yu DG, Xu L. Impact evaluations of articles in current drug delivery based on web of science. Current Drug Delivery. 2024 Mar 1;21(3):360-7.

19. Saini A, Nagar L, Panwar R, Pahwa R, Dua K, Dureja H, Verma PK. Nanostructure-based drug delivery in alleviating type 2 diabetes mellitus. BioNanoScience. 2025 Mar;15(1):177.

20. Lou J, Duan H, Qin Q, Teng Z, Gan F, Zhou X, Zhou X. Advances in oral drug delivery systems: challenges and opportunities. Pharmaceutics. 2023 Feb 1;15(2):484.

21. Rizzo F, Kehr NS. Recent advances in injectable hydrogels for controlled and local drug delivery. Advanced healthcare materials. 2021 Jan;10(1):2001341.

22. Raina N, Pahwa R, Bhattacharya J, Paul AK, Nissapatorn V, de Lourdes Pereira M, et al. Drug delivery strategies and biomedical significance of hydrogels: translational considerations. Pharmaceutics. 2022;14(3):574.

23. Chen X, Wu T, Bu Y, Yan H, Lin Q. Fabrication and biomedical application of alginate composite hydrogels in bone tissue engineering: A review. International Journal of Molecular Sciences. 2024;25(14):7810.

24. Wang Y, Shen Z, Wang H, Song Z, Yu D, Li G, Liu X, Liu W. Progress in research on metal ion crosslinking alginate-based gels. Gels. 2024 Dec 27;11(1):16.

25. Ferjaoui Z, López-Muñoz R, Akbari S, Chandad F, Mantovani D, Rouabhia M, D. Fanganiello R. Design of alginate/gelatin hydrogels for biomedical applications: fine-tuning osteogenesis in dental pulp stem cells while preserving other cell behaviors. Biomedicines. 2024 Jul 8;12(7):1510.

26. Kouchakzadeh F, Ebrahimi-Barough S, Aflatoonian B, Ai J, Mazaheri F, Montazeri F, Hajizadeh-Tafti F, Golzadeh J, Naser R, Sepehri M, Kalantar SM. Therapeutic potential of endometrial stem cells encapsulated in alginate/gelatin hydrogel to treat of polycystic ovary syndrome. Regenerative therapy. 2024 Jun 1;26:693-707.

27. Aldaghi N, Kamalabadi-Farahani M, Alizadeh M, Salehi M. Doxycycline-loaded carboxymethyl cellulose/sodium alginate/gelatin hydrogel: An approach for enhancing pressure ulcer healing in a rat model. Journal of Biomedical Materials Research Part A. 2024 Dec;112(12):2289-300.

28. Bhujbal SS, Badhe RV, Darade SB, Dharmadhikari SS, Choudhary SK. Development and Evaluation of Injectable Hydrogel as a Controlled Drug Delivery System for Metformin. Journal of Reports in Pharmaceutical Sciences. 2021 Jan 1;10(1):42-52.

29. Alpaslan D, Dudu TE, Aktaş N. Synthesis and characterization of novel organo-hydrogel based agar, glycerol and peppermint oil as a natural drug carrier/release material. Materials Science and Engineering: C. 2021;118:111534.

30. Khan R, Zaman M, Salawi A, Khan MA, Iqbal MO, Riaz R, et al. Synthesis of chemically cross-linked pH-sensitive hydrogels for the sustained delivery of ezetimibe. Gels. 2022;8(5):281.

31. Zirak Hassan Kiadeh S, Ghaee A, Mohammadnejad Arough J, Mashak A. Synthesis and Study of Lidocaine Hydrochloride from Polymeric Film as a Wound Dressing. The Journal of Shahid Sadoughi University of Medical Sciences. 2020;28(8):2934-50.

32. Borges FT, Papavasiliou G, Teymour F. Characterizing the molecular architecture of hydrogels and crosslinked polymer networks beyond Flory–Rehner—I. Theory. Biomacromolecules. 2020;21(12):5104-18.

33. Feng W, Wang Z. Tailoring the swelling-shrinkable behavior of hydrogels for biomedical applications. Advanced Science. 2023;10(28):2303326.

34. Puza F, Zheng Y, Han L, Xue L, Cui J. Physical entanglement hydrogels: Ultrahigh water content but good toughness and stretchability. Polymer Chemistry. 2020;11(13):2339-45.

35. Siboro SA, Anugrah DS, Ramesh K, Park S-H, Kim H-R, Lim KT. Tunable porosity of covalently crosslinked alginate-based hydrogels and its significance in drug release behavior. Carbohydrate Polymers. 2021;260:117779.

36. Mahmoudi C, Tahraoui Douma N, Mahmoudi H, Iurciuc CE, Popa M, Hamcerencu M, et al. Developing and characterizing a biocompatible hydrogel obtained by cross-linking gelatin with oxidized sodium alginate for potential biomedical applications. Polymers. 2024;16(22):3143.

37. Distler T, McDonald K, Heid S, Karakaya E, Detsch R, Boccaccini AR. Ionically and enzymatically dual cross-linked oxidized alginate gelatin hydrogels with tunable stiffness and degradation behavior for tissue engineering. ACS Biomaterials Science & Engineering. 2020;6(7):3899-914.

38. Ghanbari M, Salavati-Niasari M, Mohandes F, Dolatyar B, Zeynali B. In vitro study of alginate–gelatin scaffolds incorporated with silica NPs as injectable, biodegradable hydrogels. RSC advances. 2021;11(27):16688-97.

39. Lopez Hernandez H, Souza JW, Appel EA. A quantitative description for designing the extrudability of shear-thinning physical hydrogels. Macromolecular Bioscience. 2021;21(2):2000295.

40. Watt RP, Khatri H, Dibble AR. Injectability as a function of viscosity and dosing materials for subcutaneous administration. International journal of pharmaceutics. 2019;554:376-86.

41. Rył A, Owczarz P. Influence of injection application on the sol–gel phase transition conditions of polysaccharide-based hydrogels. International Journal of Molecular Sciences. 2021;22(24):13208.

42. Boffito M, Torchio A, Tonda-Turo C, Laurano R, Gisbert-Garzarán M, Berkmann JC, et al. Hybrid injectable sol-gel systems based on thermo-sensitive polyurethane hydrogels carrying pH-sensitive mesoporous silica nanoparticles for the controlled and triggered release of therapeutic agents. Frontiers in Bioengineering and Biotechnology. 2020;8:384.

43. Emami Z, Ehsani M, Zandi M, Daemi H, Ghanian M-H, Foudazi R. Modified hydroxyapatite nanoparticles reinforced nanocomposite hydrogels based on gelatin/oxidized alginate via Schiff base reaction. Carbohydrate Polymer Technologies and Applications. 2021;2:100056.

44. Ding P, Okoro OV, Sun Y, Wang L, Wei X, Liu S, et al. Graphene oxide-reinforced alginate/gelatin hydrogel via Schiff-base bond and thiol-Michael addition for bone regeneration. Materials Today Communications. 2022;33:104904.

45. Ilić-Stojanović S, Nikolić L, Nikolić V, Petrović S, Oro V, Mitić Ž, et al. Semi-Crystalline copolymer hydrogels as smart drug carriers: In vitro thermo-responsive naproxen release study. Pharmaceutics. 2021;13(2):158.

46. Salawi A, Khan A, Zaman M, Riaz T, Ihsan H, Butt MH, et al. Development of statistically optimized chemically cross-Linked hydrogel for the sustained-release delivery of favipiravir. Polymers. 2022;14(12):2369.

47. Saidi M, Dabbaghi A, Rahmani S. Swelling and drug delivery kinetics of click-synthesized hydrogels based on various combinations of PEG and star-shaped PCL: influence of network parameters on swelling and release behavior. Polymer Bulletin. 2020;77(8):3989-4010.

48. Gomaa E, Eissa NG, Ibrahim TM, El-Bassossy HM, El-Nahas HM, Ayoub MM. Development of depot PLGA-based in-situ implant of Linagliptin: Sustained release and glycemic control. Saudi Pharmaceutical Journal. 2023;31(4):499-509.

49. Abbas A, Eissa NG, El-Bassossy HM, Ghorab MM, El-Nahas HM. Polymeric linagliptin nanoparticles as a sustained release treatment for type 2 diabetes. Journal of Drug Delivery Science and Technology. 2024;93:105438.

50. Icart LP, Souza Jr FG, Lima LMT. Polymeric microparticle systems for modified release of glucagon-like-peptide-1 receptor agonists. Journal of Microencapsulation. 2021;38(4):249-61.

51. Cao B, Wang C, Guo P, Zhang Q, Wang C, Sun H, et al. Photo-crosslinked enhanced double-network hydrogels based on modified gelatin and oxidized sodium alginate for diabetic wound healing. International Journal of Biological Macromolecules. 2023;245:125528.

https://doi.org/10.22034/jrb.2026.07.V2I1A2